CORE
Metadata, citation and similar papers at core.ac.uk
Provided by DSpace@MIT

Surface Chemistry and Non-Stoichiometry of $Nd_2NiO_{4+\delta}$ Epitaxial Thin Films with Different Orientation and Strain

Nikolay Tsvetkov[a, b, †], Qiyang Lu[a,c,†], Yan Chen[a,b], and Bilge Yildiz[a,b,]

[a] Laboratory for Electrochemical Interfaces, Massachusetts Institute of Technology, Cambridge, MA 02139, USA
[b] Department of Nuclear Science and Engineering, Massachusetts Institute of Technology, Cambridge, MA 02139, USA
[c] Department of Materials Science and Engineering, Massachusetts Institute of Technology, Cambridge, MA 02139, USA
[†] These authors contributed equally

The influence of lattice strain on non-stoichiometry and surface chemical composition was investigated for epitaxial $Nd_2NiO_{4+\delta}$ (NNO) films during annealing in ultra high vacuum (below 10^{-8} mbar) and temperatures of up to 700°C. (100)- and (001)-oriented films with tensile and compressive lattice strain along c-axis were fabricated using pulsed laser deposition method. A significant decrease in the c-lattice parameter during annealing was found by x-ray diffraction (XRD) for the tensile strained films. X-ray photoelectron spectroscopy (XPS) showed that Ni reduction during annealing takes place only in compressively strained films, indicating the lower content of oxygen interstitials. A lower interstitial content in the compressively strained NNO films is consistent with the smaller c-lattice parameter measured by XRD and the easier reducibility of Ni measured by XPS. Cation segregation and morphological changes were found only for the compressively strained film surfaces. These results show that lattice strain along the c-axis is an important parameter that can alter the surface chemistry, and thus the oxygen exchange kinetics, on $Nd_2NiO_{4+\delta}$ at elevated temperatures.

Introduction

One of the major barriers to achieve solid oxide fuel cells (SOFCs) with high power output at intermediate (500-700°C) temperature is the slow oxygen reduction (OR) rate at the cathode (1). Understanding the fundamental aspects of fast oxygen transport and electro-catalytic activity at moderate temperatures in oxides is a key for designing high performance electrodes in solid oxide fuel cells (SOFCs), gas sensors, and separation membranes (1-5). Particularly important is the ability to tune at the atomic-level structural, chemical, and electronic properties of the oxide surfaces and interfaces (6). However, generalized theoretical and experimental strategies for this purpose are scarce. One challenge has been the modeling and manipulation of ionic and electronic transport in poly-crystalline electrodes with irregular microstructure. The use of epitaxial oxide thin films cathodes allows one to isolate the effects of crystal orientation and strain on the OR and ionic transport kinetics.

Downloaded on 2013-11-25 to IP 18.189.31.95 address. Redistribution subject to ECS license or copyright; see ecsdl.org/site/terms_use

Surface strain effects have received significant interest for low temperature electrocatalysis on transition metals since the report by Mavrikakis et al.[7] The investigations focused on the differences in reactivity based on the strain-driven atomic arrangements of surface atoms, which may include compressed or expanded configurations (7,8), and the vicinity of extended defects such as dislocations and step edges (9). In the field of SOFC, only recent investigations demonstrated the favorable effects of lattice strain. Cai et al. discovered that the electronic structure of $La_{0.6}Sr_{0.4}CoO_{3-\delta}$(LSC) thin films can be strongly correlated to the strain types and the tensile strain can enhance charge transfer on the surface (10). Moreover, Kubicek et al.'s 18O exchange measurements on the same LSC/$SrTiO_3$ and LSC/$LaAlO_3$ samples, with different strain types clearly showed that tensile lattice strain can accelerate the oxygen surface exchange and diffusion kinetics in LSC thin films (11).

The effects of strain can be more pronounced in materials with anisotropic structure such as oxygen excess Ruddlesden-Popper (RP) family, K_2NiF_4. Its structure is an archetypal complex oxide which consists of two different layers, a rock salt layer separating the perovskite blocks.

Conventionally, cubic symmetry solids, such as perovskites and fluorites, are materials which are used for SOFC application. In these materials the oxygen ion conduction takes place by the thermally activated hopping of ions via the vacant lattice sites. The oxygen molecular adsorption and dissociation on the surfaces are also mediated by the oxygen vacancies. Unlike these conventional materials, in RP oxides the oxygen species intercalate through interstitial positions on the surface (12). Moreover according to theoretical calculations, the oxygen diffusion coefficient in the RP oxides increases with increase in oxygen over-stoichiometry up to a certain level (13).

The surface chemistry and electronic structure, which are important determinants of cathode OR activity, are not yet elucidated in general on RP oxides. In this work, we have chosen Nd_2NiO_4 (NNO) as the model RP material because of its high oxygen diffusion and surface exchange coefficients (14). At the moment there are only few works on epitaxial NNO films in application as SOFC cathode (15,16) and no prior investigation about the effect of strain on the defect chemistry, surface chemistry and OR reactivity has been reported.

In this study, we focus on the impact of lattice strain and crystal orientation on surface electronic structure and the chemical state of the NNO oxide thin films at elevated temperature.

Experiments

Oxide target that was used for pulsed laser deposition (PLD) was prepared by the conventional Pechini method starting from neodymium and nickel nitrates powders. The obtained $Nd_2NiO_{4+\delta}$ has an orthorhombic unit cell with a=5.374 Å, b=5.458 Å and c=12.387 Å, which can be characterized in term of a pseudocubic-lattice constant with $a_{pc}\approx b_{pc}\approx 3.84$ Å. PLD was used to fabricate NNO films with thickness of around 20 nm on four different substrates: $SrLaAlO_4$(100) (SLAO), $NdCaAlO_4$(100) (NCAO), $SrTiO_3$(001) (STO), $LaAlO_3$(001) (LAO). PLD was performed using a KrF excimer laser

Downloaded on 2013-11-25 to IP 18.189.31.95 address. Redistribution subject to ECS license or copyright; see ecsdl.org/site/terms_use

with wavelength of 248 nm. The films were deposited at 700 ^{o}C under oxygen pressure of 10 mTorr. After the growth process, the films were cooled down to room temperature in 10 Torr oxygen pressure to oxidize the films.

Crystal structure of the prepared target was investigated using PANalytical X'Pert Pro multipurpose diffractometer using Cu $K\alpha_1$ radiation. Crystal structure and strain state of thin films were identified using Rigaku Smartlab diffractometer equipped with 2-bounce Ge (220) channel-cut monochromator using Cu $K\alpha_1$ radiation. The morphology of the films were investigated by scanning electron microscopy (SEM) using a Helios NanoLab 600 DualBeam microscope.

In situ X-ray photoelectron spectroscopy (XPS) measurements have been performed in order to investigate the effects orientation and strain on surface chemistry as a function of temperature during annealing in vacuum. In order to clean the surface form the carbon related contamination the films were annealed in oxygen partial pressure of 10^{-5} mbar and temperature of 450 ^{o}C during 1 hour. The XPS data collected at different electron emission angles allows to quantify the surface chemical composition with near-surface resolution. The Nd 4d, O 1s, and Ni 2p emissions were measured and used in the analysis. For the excitation energy of 1486.48 eV, the sampling depths of these photoelectrons at emission angle $\varphi=0°$ are ∼6 nm for Nd 4d, ∼3 nm for Ni 2p, and ~ 4 nm for O 1s. At the emission angle $\varphi=60°$, the measurements are more surface sensitive, since the sampling depths of each element are half of those at the emission angle of 0°.

Annealing of the samples was performed within XPS analysis chamber under ultra-high vacuum (UHV) conditions in the temperature range of 400-700 ^{o}C. During the annealing the pressure was kept below 10^{-8} mbar.

Results and Discussion

Orientation and Substrate-Induced Lattice Strain

Figure 1 shows high-resolution x-ray diffraction (HRXRD) 2θ-ω scan patterns used to characterize the orientation and out-of-plane parameters of the thin film samples. From the HRXRD results it can be noted that the NNO thin films on SLAO and NCAO substrates (Fig. 1a) demonstrates only (h00) diffraction peaks, indicating the ab-plane is perpendicular to the substrate surface. Only (00k) peaks were detected in the HRXRD pattern of NNO thin films on STO and LAO substrates (Fig. 1d), indicating that ab-plane is parallel to the substrate surface. The schematic representation of substrate induced strain states is also given in Figure 1.

Based on the results of HRXRD analysis we conclude that all NNO are epitaxial and are fully strained with the substrate. The out-of-plane lattice parameters were calculated using the Bragg equation. The in-plane and out-of-plane lattice parameters and corresponding strain for all four thin samples are listed in Table 1.

It should be noted that the c-lattice parameter in Ruddlesden-Popper phase materials is responsible for the distance between the perovskite blocks and related with the degree of oxygen non-stoichiometry, δ; the larger the c, the larger the +δ (17). Thus, we can

Downloaded on 2013-11-25 to IP 18.189.31.95 address. Redistribution subject to ECS license or copyright; see ecsdl.org/site/terms_use

expect higher oxygen interstitial content for the films with tensile strain along the c-axis (NNO/LAO and NNO/SLAO, tensile strained films) than for the films with compressive strain along the c-axis (NNO/STO and NNO/NCAO, compressively strained films).

TABLE 1. Estimated in-pane, calculated out-of-plane lattice parameters, and corresponding strain states in NNO films on various substrates.

Lattice parameter	$Nd_2NiO_{4.19}$	(100)NNO/ NCAO	(100)NNO/ SLAO	(001)NNO/ STO	(001)NNO/ LAO
a_{pc}	3.84 Å	3.66 Å* (-4.7%)	3.76 Å* (-2.1%)	3.91 Å (1.8%)	3.82 Å (-0.5%)
c	12.21 Å	12.12 Å (-0.7%)	12.63Å (3.4%)	12.19 Å* (-0.2%)	12.41 Å* (1.6%)

* out-of-plane lattice parameter

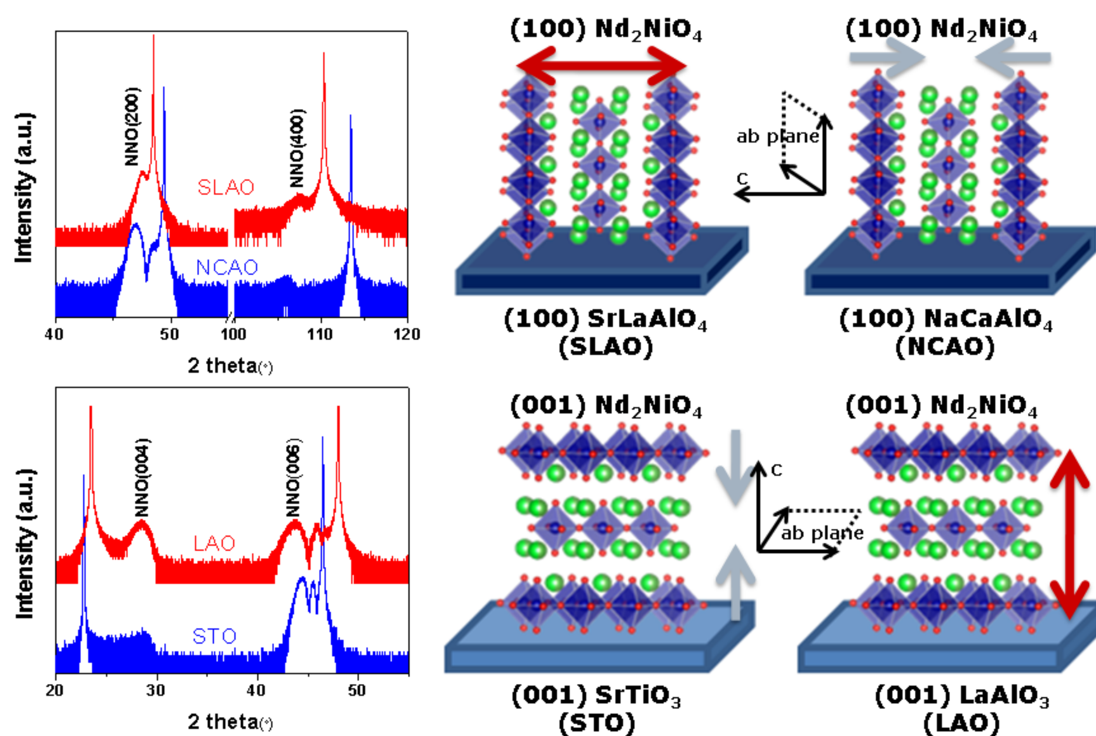

Figure 1. HRXRD patterns of NNO thin films with (a) (100) and (b) (001) orientations. The substrate induced strain types in different directions are shown schematically.

Change in Lattice Parameters during Annealing

The effect of annealing in UHV on lattice parameters of NNO thin film was investigated for tracing the effects of strain and orientation on oxygen non-stoichiometry. The comparative HRXRD patterns of as-prepared and annealed films are shown in Figure 2. The changes of out-of-plane lattice parameters induced by UHV annealing are summarized in Figure 3.

The HRXRD measurements have shown that during annealing under UHV conditions there is a significant change in the out-of-plain lattice parameter for the tensile strained

Downloaded on 2013-11-25 to IP 18.189.31.95 address. Redistribution subject to ECS license or copyright; see ecsdl.org/site/terms_use

films. At the same conditions, very little change in the out-of-plane lattice parameter was observed for the compressively strained films.

For the films with (001) orientation the observed result can be reasonably attributed to the significant loss of oxygen interstitials during the annealing in vacuum. It can be related with the higher initial δ and to the fast oxygen out-diffusion in the tensile strained films. Compressively strained film, on the other hand, is expected to have a lower initial δ, and shows only a small decrease in c-lattice parameter and δ in comparison to that for the tensile strained films.

Similar effect of annealing on δ was found for films with (100) orientation. Films with tensely strain along c-axis show significant increase in a-lattice parameter indicating the significant decrease in δ (17). At the same time the change of a-lattice parameter and δ is much smaller for compressively strained films.

Thus, we can conclude that the film strain, but not the orientation, primarily affects the change in the lattice parameters and δ during annealing.

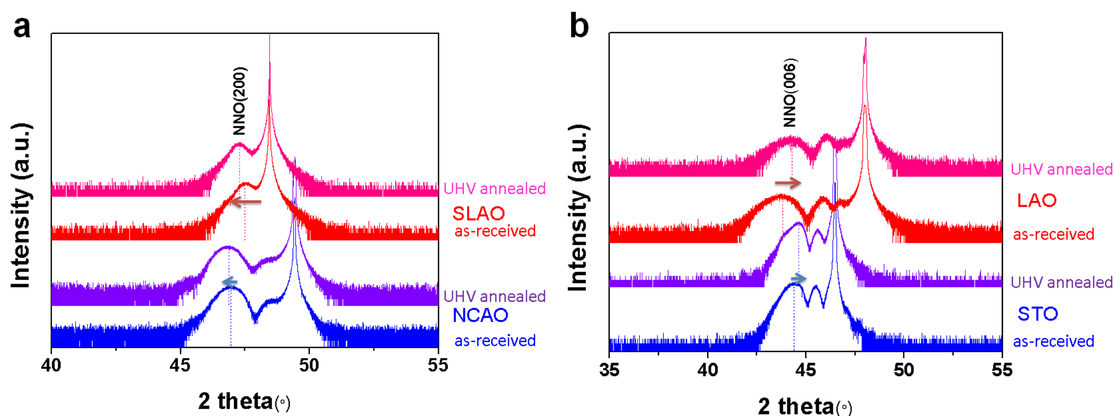

Figure 2. HRXRD patterns of the NNO thin films in their as-received condition and upon annealing in UHV conditions at 700 ^{o}C, for: (a) (100) and (b) (001) orientation.

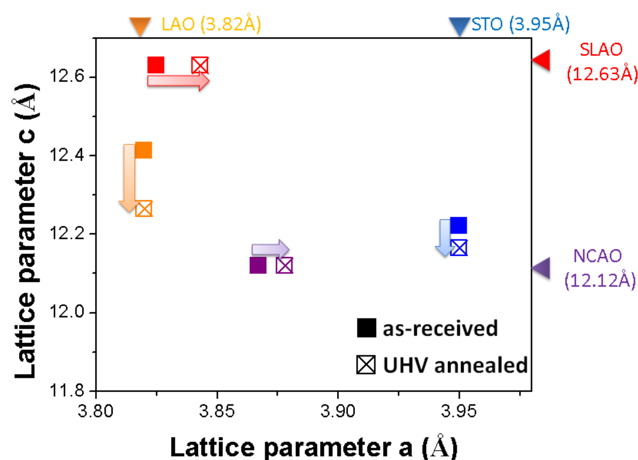

Figure 3. Change of the out-of-plane lattice parameter of NNO films on various substrates upon annealing in UHV conditions at 700 ^{o}C.

Downloaded on 2013-11-25 to IP 18.189.31.95 address. Redistribution subject to ECS license or copyright; see ecsdl.org/site/terms_use

Evolution of the Ni Oxidation State during Annealing

The explanation of the phenomena observed by XRD requires also tracing the change in the electronic structure of the films during UHV annealing. This can be performed in-situ using XPS. XPS was used to estimate the change of the cation oxidation state and chemical composition on the surface during UHV annealing.

No detectable change in the spectrum shape for Nd 4d peaks was observed for all the films within the all temperature range (data not shown). Based on this result we can conclude that there was no change in the oxidation state of Nd.

Figure 4a shows the typical spectra of Ni 2p peaks from NNO films with different crystal orientations and strain types annealed in UHV at different temperatures. The effect of annealing in vacuum can be characterized based on the analysis of the shape of Ni peak. For both the (001)- and (100)-oriented tensile strained NNO films Ni 2p peaks do not show any measurable changes, indicating the similar oxidation state (mainly Ni^{2+}) at all the temperatures in the range under investigation.

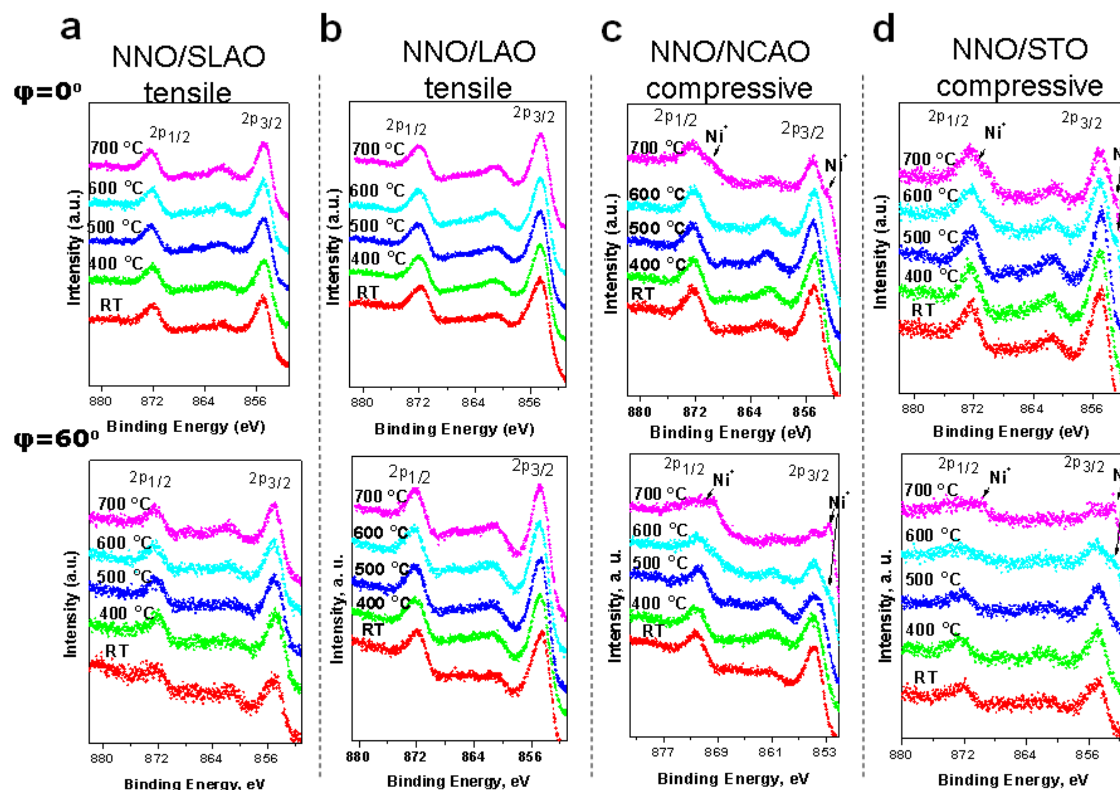

Figure 4. The Ni 2p photoelectron spectra recorded from (a) NNO/SLAO, (b) NNO/LAO, (c) NNO/NCAO, and (d) NNO/STO films at (a) 0° (top) and 60° (bottom) emission angle.

For the compressively strained NNO films the Ni 2p spectra changes significantly as a function of temperature. The formation of extra peaks in the lower binding energy can be clearly seen. Considering that the main oxidation state of Ni in the NNO is Ni^{2+}, the additional emission in the lower binding energy side can be reasonably assigned to Ni^{+}. Given that in the stoichiometric Nd_2NiO_4, the Ni^{2+} corresponds to the state when no

Downloaded on 2013-11-25 to IP 18.189.31.95 address. Redistribution subject to ECS license or copyright; see ecsdl.org/site/terms_use

oxygen interstitials are present, the appearance of Ni^+ shows that oxygen vacancies are the dominant oxygen non-stoichiometric species on the sample surface.

The Ni^+ peak became more pronounced in the XPS spectra obtained at 60° emission angle (Fig. 4b). This result points out that the formation of oxygen vacancies takes place primarily at/near the surface of the compressively strained NNO films.

Evolution of the Surface Chemical Composition during Annealing

The results of quantitative analysis of surface compositions for NNO films with different strain and orientation annealed at different temperatures under UHV conditions are summarized in Figure 5.

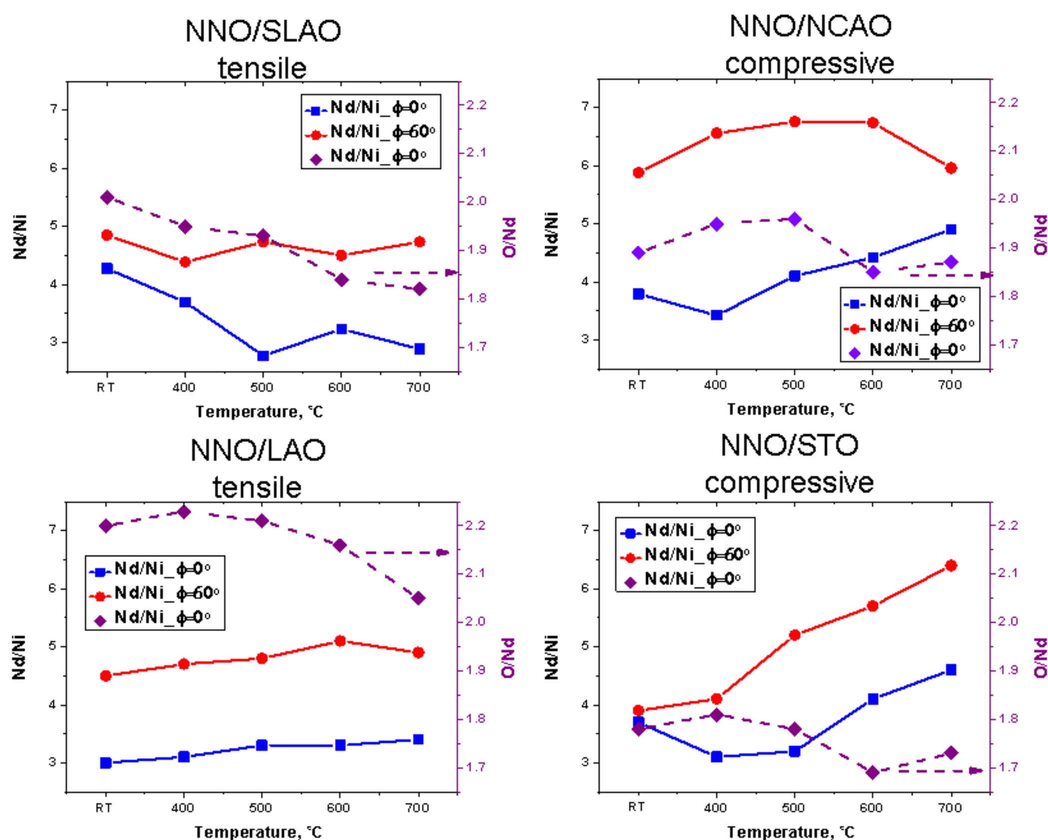

Figure 5. Nd/Ni and O/Nd ratios for NNO films on various substrates.

Nd and O Content on the Surface

Analysis of O/Nd ratio showed that the oxygen content decreased significantly in tensile strained samples during UHV annealing. The decrease in O content during annealing can be attributed to the decrease in δ and is in line with the shrinkage of c-lattice parameter observed during XRD measurements. On the other hand, O/Nd ratio, as well as the c-lattice parameter, remains almost the same for compressively strained films. In compressively strained films, Ni is easier to reduce due to lower amount of initial δ. No significant change of lattice parameters was observed because vacancy formation at the film surface.

Downloaded on 2013-11-25 to IP 18.189.31.95 address. Redistribution subject to ECS license or copyright; see ecsdl.org/site/terms_use

For tensile strained films the large decrease in the O/Nd ratio is in line with observed significant lattice shrinkage related with the significant decrease in δ.

All the films under investigations possess some amount of oxygen interstitials which are lost partially during UHV annealing. However, almost for all the samples initial O/Nd ratio was found to be below 2. This can be related with the presence of Nd-rich phase at the film surface (see below). The exact nature of the surface layer of RP phase materials is still under discussion, however it is commonly accepted that the surface segregation involves an A-site cation rich compound (18). For Nd_2NiO_4, in the extreme case, it can be Nd_2O_3 with an O/Nd ratio of 3/2, which would lead to a hypo-stoichiometric value of O/Nd when measured by a near-surface technique like XPS.

Ni and Nd Content on the Surface

All the NNO films show significant increase in Nd/Ni ratio at the electron emission collection angle of 60° in compare to angle of 0°. This result indicates that the Nd segregation takes place at the film surface.

We have found that the Nd segregation at the film surface depends primarily on the strain type rather than the film orientation. The tensile strained NNO films show almost unchanged Nd/Ni ratio in the temperature range under investigation. At the same time the compressively strained films demonstrate the increase in the Nd/Ni ratio during annealing.

It should be noted that the decrease in Nd/Ni ration for NNO/NCAO sample at 700 ^oC is likely due to the formation of significant surface irregularities (see below). According to our previous studies, high surface roughness due to agglomeration of surface segregation leads to an underestimate of the segregated cation when measured by the near-surface technique XPS (18).

Evolution of Surface Morphology

The process of the surface composition change during reduction can lead to the change of the film morphology. The scanning electron microscopy was applied to study the evolution of the NNO morphology depending on the film strain and orientation.

Figure 7 shows surface morphology on NNO films with different strain type and orientations before and after annealing under UHV conditions. For all the films before annealing smooth surfaces without any significant defects can be observed.

Almost no changes were detected after UHV annealing in the case of tensile strained films.

For the compressively strained films which demonstrate Nd segregation during annealing under UHV conditions, significant changes in the surface morphology was observed. In the case of (100) NNO/NCAO film the particles with the diameter of around 10 nm can be observed at the film surface. Regarding the results of chemical composition analysis it is reasonable to propose that these particles consist of Nd-reach phase segregated during annealing process. For the (001) NNO/STO the formation of the hole

Downloaded on 2013-11-25 to IP 18.189.31.95 address. Redistribution subject to ECS license or copyright; see ecsdl.org/site/terms_use

at the film surface was observed. These holes are surrounded by small particles with the diameter around 2-3 nm (Figure 7, insert).

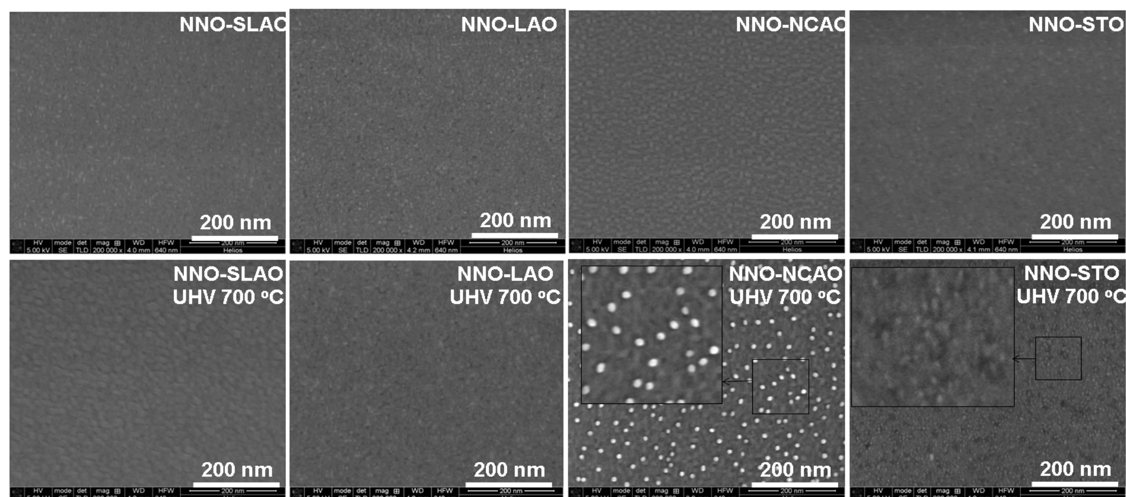

Figure 7. Surface morphology NNO films before and after annealing under UHV conditions.

We hypothesize that the elastic energy minimization is a driver for Nd segregation. We propose that Ni reduction leads to increase of ionic radius of Ni and consequently to the increase in the size of perovskite block (19). Enlarging on perovskite layers stresses the rock salt layer and can lead to driving out of the relatively large Nd atoms to the surface in order to minimize elastic energy of the system.

Conclusion

The experimental results obtained on tensile and compressive $Nd_2NiO_{4+\delta}$ films demonstrate how substrate-induced lattice strain can affect non-stoichiometry, transition metal oxidation state, electronic structure as well as surface chemical composition and morphology of RP oxide thin films. The substrate induced strain along the c-axis, rather than the crystal orientation, primarily determines the oxygen non-stoichiometry of the NNO oxide thin films. The NNO films with compressive strain along the c-axis are more reducible compared to the tensile strained films. Nd segregation and surface morphology changes during annealing under UHV conditions are more evident for the films on the NNO films with compressive strain along the c-axis. We attribute this to the elastic energy minimization along the rock-salt layers that is compressively stressed.

In this work, the strain response of RP phase represented by the model $Nd_2NiO_{4+\delta}$ composition was found to be anisotropic, and the strain along the c-axis was found to be a key parameter to altering the non-stoichiometry and surface chemistry. These results have important implications to surface oxygen exchange which is currently being investigated on these films.

Downloaded on 2013-11-25 to IP 18.189.31.95 address. Redistribution subject to ECS license or copyright; see ecsdl.org/site/terms_use

Acknowledgments

The authors acknowledge the funding support from the CAREER Award of the National Science Foundation, Division of Materials Research, Ceramics Program. The authors also acknowledge the use of the Center for Materials Science and Engineering, an MRSEC facility of NSF at MIT.

References

1. B.C.H. Steele, *Mater. Sci. Eng*. B, **13,** 79 (1992).
2. Z. P. Shao and S. M. Haile, *Nature*, **431**, 170 (2004).
3. N. Q. Minh, *J. Am. Ceram. Soc*., **76**, 563 (1993).
4. Z. Zhan, W. Kobsiriphat, J. R. Wilson, M. Pillai, I. Kim, and S. A. Barnett, *Energy Fuel*, **23**, 3089 (2009).
5. H. L. Tuller, S. J. Litzelman, and W. Jung, *Phys. Chem. Chem. Phys*., **11**, 3023 (2009).
6. S. J. Litzelman, J. L. Hertz, W. Jung, and H. L. Tuller, *Fuel Cells*, **8**, 294 (2008).
7. M. Mavrikakis, B. Hammer, and J. K. Norskov, *Phys. Rev. Lett.,* **81**, 2819 (1998).
8. M. Mavrikakis, P. Stoltze, and J. K. Norskov, *Catal. Lett*., **64**, 101 (2000).
9. Y. Xu and M. Mavrikakis, *J. Phys. Chem*. B, **107**, 9298 (2003).
10. Z. Cai, Y. Kuru, J. W. Han, Y. Chen, and B. Yildiz, *J. Amer. Chem. Soc*., **133**, 17696 (2011).
11. M. Kubicek, Z. Cai, W. Ma, B. Yildiz, H. Hutter, and J. Fleig, *ACS Nano*, **7,** 3276 (2013).
12. W. Paulus, A. Cousson, G. Dhalenne, J. Berthon, A. Revcolevschi, S. Hosoya, W. Treutmann, G. Heger, and R. Le Toquin, *Solid State Sci.*, **4**, 565 (2002).
13. D. Parfitt, A. Chroneos, J. A. Kilner, and R. W. Grimes, *Phys. Chem. Chem. Phys*., **12**, 6834 (2010).
14. F. Mauvy, C. Lalanne, S. Fourcade, J. M. Bassat, and J. C. Grenier, *J. Eur. Ceram. Soc*., **27**, 3731 (2007).
15. A. Yamada, Y. Suzuki, K. Saka, M. Uehara, D. Mori, R. Kanno, T. Kiguchi, F. Mauvy, and J. C. Grenier, *Adv. Mater*., **20**, 4124 (2008).
16. A. Yamada, K. Saka, M. Uehara, S. Taminato, R. Kanno, F. Mauvy, and C. Grenier, *Electrochem. Comm*., **12**, 1690 (2010).
17. T. Nakamura, K. Yashiro, K. Sato, and J. Mizusaki, *Solid State Ionics*, **181**, 402 (2010).
18. W. Lee, J. W. Han, Y. Chen, Z. Cai, and B. Yildiz, *J. Am. Chem. Soc*., **135**, 7909 (2013).
19. Y. Kuru, D. Marrocchelli, S. R. Bishop, D. Chen, B. Yildiz, and H. L. Tuller, *J. Electrochem. Soc*., **159**, F799 (2012).

Downloaded on 2013-11-25 to IP 18.189.31.95 address. Redistribution subject to ECS license or copyright; see ecsdl.org/site/terms_use